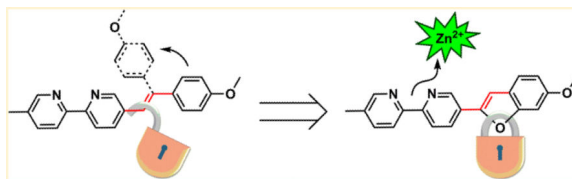# Enhancing the Photostability of Arylvinylenebipyridyl Compounds as Fluorescent Indicators for Intracellular Zinc(II) Ions

**Zhao Yuan**[†], **Ali H. Younes**[†,#], **John R. Allen**[‡], **Michael W. Davidson**[*,‡], and **Lei Zhu**[*,†]

[†]Department of Chemistry and Biochemistry, Florida State University, 95 Chieftan Way, Tallahassee, Florida 32306-4390, United States

[‡]National High Magnetic Field Laboratory and Department of Biological Sciences, Florida State University, 1800 East Paul Dirac Drive, Tallahassee, Florida 32310, United States

## Abstract



Arylvinylenebipyridyl (AVB) ligands are bright, zinc(II)-sensitive fluoroionophores. The applicability of AVBs as fluorescent indicators for imaging cellular zinc(II), however, is limited by low photostability, partially attributable to the photoisomerization of the vinylene functionality. Two configurationally immobilized (i.e., "locked") AVB analogues are prepared in this work. The zinc(II)-sensitive photophysical properties and zinc(II) affinities of both AVBs and their locked analogues are characterized in organic and aqueous media. The zinc(II) sensitivity of the emission is attributed to the zinc(II)-dependent energies of the charge transfer excited states of these compounds. The configurationally locked ligands have improved photostability, while maintaining the brightness and zinc(II) sensibility of their AVB progenitors. The feasibility of the "locked" AVB analogues with improved photostability for imaging intracellular Zn(II) of eukaryotic cells using laser confocal fluorescence microscopy is demonstrated.

## INTRODUCTION

Zinc(II) ions are involved in a broad spectrum of mammalian physiological processes.[1–3] The amount of kinetically labile (sometimes referred as "free") zinc(II) in an organism is

maintained in a delicate homeostatic balance,[4–6] the deviation from which is implicated in many diseases.[7,8] The understanding, on the cellular and molecular levels, of the functions of zinc(II) in these disease-causing processes is expected to aid diagnosis and treatment. An indicator that is capable of selectively recording zinc(II) abundance and trafficking in living cells in preferably a quantitative manner would be an invaluable tool in zinc(II) biology. The choice of fluorescence as the signal readout is attributed to the minimally invasive live-cell imaging capabilities and the ever-increasing spatial and temporal resolutions of modern fluorescence microscopes.[9] The success of fluorescent calcium(II) indicators[10,11] is a significant facilitator in the development of zinc(II) indicators, by providing valuable experience in the design of ligands and fluorophores.

Zinc(II) indicators[12–16] based on fluorescence intensity readout can be separated into two categories.[17,18] A fluorescence turn-on indicator reports the zinc(II) concentration by a proportional increase in fluorescence intensity without changing its frequency. The fluorescence intensity at a single wavelength therefore is a function of zinc(II) concentration. A fluorescence ratiometric indicator undergoes zinc(II)-dependent emission frequency change without significantly altering the fluorescence quantum yield. Therefore, the zinc(II) concentration is the function of the ratio of emission intensity at two wavelengths, those of the free and zinc(II)-bound indicators. A ratiometric readout is sometimes preferred over the absolute intensity readout of a turn-on indicator, because the output dependence on photobleaching and uneven loading of dyes as well as on instrumental variations are somewhat minimized in the ratiometric mode.[10,19]

From a molecular design point of view, turn-on and ratiometric indicators require different structural considerations. A turn-on indicator is a fluorophore of which the major nonradiative decay pathway is eliminated upon forming a zinc(II) complex, while the wavelength of emission is unchanged. For a ratiometric indicator, the ground- and excited-state energies are altered differently upon binding zinc(II), thus resulting in an emission frequency change. A straightforward method for creating a ratiometric indicator is to exploit the differing electrostatic interactions between a zinc(II) ion and ground- and excited-state dipoles of a charge-transfer fluorophore (also commonly referred to as a donor—acceptor, or a "push-pull" fluorophore). Assuming the excited state has a dipole moment larger than that of the ground state, cation coordination at either the positive or the negative end of the excited-state dipole (or the disjoint HOMO or LUMO orbital in a quadruple[20,21]) would lead to a hypsochromic or a bathochromic shift, respectively, of emission and/or excitation (Figure 1). Other frequency- changing molecular photophysical processes such as excimer formation, excited-state proton transfer, and Förster resonance energy transfer can also be rendered zinc(II)-dependent for creating ratiometric zinc(II) indicators.[15,16]

Our group has studied the fluorescence properties of arylvinylenebipyridyl (AVB) compounds, which are considered charge-transfer fluorophores.[22,23] An example is compound **1** (Chart 1), which has a *p*-methoxyphenyl as the electron-donating group that is conjugated via a vinylene functionality to the electron-withdrawing bipyridyl. The push–pull AVBs show a positive emission solvatochromic effect, and bathochromic shifts in both emission and excitation upon zinc(II) binding at the bipyridyl site. Despite the brightness and zinc(II) sensitivity of the AVBs, such as **1** and **3** (Chart 1),[22] one drawback of this series

of compounds is the lack of photostability resulting from their propensity for photoisomerization. To address this issue, compounds **2** and **4** (Chart 1) are prepared in the current work, in which the vinylene trans configurations are frozen in a furan ring. As a result, the zinc(II) sensitivity of their AVB precursors **1** and **3** is preserved, while the photostability is improved.

## RESULTS AND DISCUSSION

### 1. Synthesis

The synthesis of compound **2** is shown in Scheme 1. Horner–Wadsworth–Emmons reaction between aldehyde **2**[24] and diethyl phosphonate **6**[25] afforded compound **7** in 80%. Removal of the methoxymethyl (MOM) group of **7** by TsOH resulted in compound **8**, which upon treating with $I_2$ in the presence of $K_2CO_3$ was converted to compound **2**.[26]

The synthesis of compound **4** is outlined in Scheme 2. Compound **11**[27] was prepared from the commercially available 3-methoxythiophene (**9**) in two steps. Protection of the hydroxy group of **11** by methoxymethyl bromide (MOMBr) afforded aldehyde **12** in 95%, which underwent the Horner–Wadsworth–Emmons reaction with diethyl phosphonate **6**[25] to give compound **13** in 66%. The MOM group of compound **13** was removed using TsOH to result in **14**, the oxidative cyclization of which using $K_2CO_3$ and $I_2$ afforded compound **4**.

### 2. Solvent-Dependent Fluorescence of Compounds 2 and 4

Apart from the reinforced trans-configuration in a furan ring, the structure of compound **2** is similar to that of **1**. The fluorescence quantum yield ($\varphi$) and lifetime ($\tau$) of compounds **1** and **2** were measured in different solvents (Table 1). The time constants of radiative ($k_r$) and nonradiative ($k_{nr}$) decays (Table 1) were calculated based on eqs 1 and 2. The $\varphi$ and $\tau$ values of the configurationally immobilized compound **2** are larger than those of the photoisomerizable **1**, by 90% and 100% on average, respectively. Both compounds have similar $k_r$ values in the same solvents. However, compound **2** has significantly smaller $k_{nr}$ than that of **1** in all solvents. These data suggest that the configurational stability of **2** does not contribute to a more allowed radiative transition (a larger $k_r$). Rather, the rate of nonradiative decay is reduced (a smaller $k_{nr}$, by 78% on average), most likely a consequence of eliminating the photoisomerization pathway.

$$k_r = \frac{\phi}{\tau} \quad (1)$$

$$k_{nr} = \frac{1 - \phi}{\tau} \quad (2)$$

It is noteworthy that the high fluorescence quantum yield ($\varphi$) of compound **2** measured in organic solvents ( 0.69) depends little on solvent polarity. The lifetime ($\tau$) of **2** increases moderately as the solvent polarity grows, which can be attributed to the increasing charge-transfer character of the emissive excited state that likely decreases $k_r$. The substantial excited-state dipole moment of compound **2** is reflected in the solvent-dependent emission

band shape and wavelength (Figure 2a). A structured fluorescence spectrum was obtained in the nonpolar hexanes, which do not offer strong solvent–solute interactions that would lead to inhomogeneous broadening of the spectrum.[28,29] As the polarity and/or the hydrogen bond donating ability of the solvent increases, the strong solvent–solute interaction not only stabilizes the dipolar excited state of **2** but contributes to the inhomogeneous broadening, to result in a broad, structure-less emission at a longer wavelength from that in hexanes. The normalized excitation of **2** in all solvents is independent of emission wavelength (Figures S1–S5, Supporting Information), which indicates that solvent relaxation of the excited state is fast and reaches equilibrium well within the lifetime of the excited fluorophore. On the basis of the literature convention, the structured high energy emission of **2** in hexanes might be referred to as the locally excited (LE) emission, whereas the structure-less low energy emission in more polar solvents is considered to be charge transfer (CT) emission, although the meanings of LE and CT could become ambiguous under different contexts.[30–33] The emission of compound **4** has similar solvent dependency, the spectra of which are shown in Figure 2b.

The φ and τ values of compounds **3** and **4** along with the $k_r$ and $k_{nr}$ values are listed in Table 2. The $k_r$ values of the configurationally locked **4** in the tested solvents are larger than that of the "unlocked" olefin analogue **3**. The rates of nonradiative decay ($k_{nr}$) of **4** are significantly smaller than those of **3** in all solvents. These observations are consistent with the comparison between compounds **1** and **2** and support the rationale that eliminating the potential of photoisomerization in the AVB fluoroionophores by confining the trans double bond in a heterocycle decreases the rate of nonradiative decay, hence increasing the fluorescence quantum yield.

### 3. Fluorescence Titrations of 1–4 with Zn(ClO$_4$)$_2$ in CH$_3$CN

The fluorescence quantum yields, lifetime, and emission maxima of compounds **1–4** under zinc(II)-free and zinc(II)-saturated conditions in CH$_3$CN are listed in Table 3. Similar to their configurationally unlocked olefin counterparts, the binding of zinc(II) (in the form of Zn(ClO$_4$)$_2$) of the locked CT fluoroionophores **2** and **4** in CH$_3$CN leads to bathochromic shifts of their absorption and emission spectra (Figures S6 and S7, Supporting Information). As an example, the zinc(II) titration data using compound **4** in both absorption and emission modes are included as Figure S9, Supporting Information. Both lowest energy absorption and emission bands of **4** were red-shifted as zinc(II) titration proceeded. Therefore, this compound could be used for analyzing zinc(II) in a ratiometric mode, i.e., the ratio of the absorption or the emission bands of the zinc(II)-free and the zinc(II)-bound forms, respectively, is a function of zinc(II) concentration. The *p*-methoxyphenyl-containing compounds **1** and **2** are capable of larger zinc(II)-induced emission bathochromic shifts ($\Delta\tilde{\nu}_{em}$, Table 3) than the thienyl-containing **3** and **4**, suggesting that the *p*-methoxyphenyl group is a more effective electron-donating group than the thienyl in CT type fluorophores. Fluorescence quantum yield (φ) relates to the rates of both radiative ($k_r$) and nonradiative ($k_{nr}$) decays (eq 3). Unlike compounds **1** and **3**, the φ values of which grow upon zinc(II) binding due to a more significant decrease in $k_{nr}$ relative to $k_r$ (Table 3), the metal-free forms of compounds **2** and **4** already have high fluorescence quantum yields, which are slightly reduced upon zinc(II) binding, attributable to the steeper drop of $k_r$ relative to $k_{nr}$ (Table 3).

$$\phi = \frac{k_r}{k_r + k_{nr}} \quad (3)$$

## 4. Fluorescence Titrations of 1–4 with Zn(ClO$_4$)$_2$ under Physiologically Relevant Conditions

The zinc-(II)-dependent fluorescence of **1–4** was also studied under simulated physiological conditions to evaluate the applicability of these ligands in imaging zinc(II) ions in biological systems.[12–16] The zinc(II)-dependent emission wavelengths and quantum yields of **1–4** are listed in Table 4. In a neutral aqueous solution (see caption of Figure 3), the emission maximum of **2** (478 nm, φ = 0.25) appears at a longer wavelength than that of **1** (460 nm). The free ligand **1** has a fluorescence quantum yield (φ) of 0.05. The titration of Zn(ClO$_4$)$_2$ leads to the formation of bipy/zinc(II) complex, which at saturation results in a φ of 0.31 along with a red shift of 53 nm ($\Delta \tilde{\nu}_{em}$ = 2,246 cm$^{-1}$) of compound **1**. Under the same conditions, the zinc(II) complex of the configurationally rigid **2** had a longer emission band (524 nm, φ = 0.15) with a smaller zinc(II)-effected bathochromic shift (46 nm; 1,837 cm$^{-1}$).

Excited at 405 nm where the zinc(II) complex preferentially absorbs, the zinc(II)-dependent emission spectra of **2** acquired under different conditions are shown in Figure 3. The emission spectra of **1, 3**, and **4** are included in the Supporting Information (Figures S10–S12). A largely emission enhancement, instead of a ratiometric change, as [zinc(II)] increases was observed due to the increased absorption from the zinc(II) complex at the excitation wavelength of 405 nm.[34] The intensity at the emission maxima was plotted versus the free zinc(II) concentration [Zn]$_f$ (see insets of Figure 3) for assessing the zinc(II) affinity of **2**. The [Zn]$_f$ values were controlled using a ligand at millimolar with known zinc(II) affinity (a "metal buffer").[35] In this case, three metal buffers were evaluated for their appropriateness in determining the affinity of the ligands to zinc(II), as measured by the apparent 1:1 dissociation constant ($K_d$).[36] Using nitrilotriacetic acid (NTA, $K_d$(Zn) = 14 nM) as the metal buffer, the emission of compound **2** (Figure 3a) grew with increasing [Zn]$_f$. However, when the upper limit of the NTA buffering range was reached, the emission of **2** was not yet half saturated, as marked by the red curve. A similar observation was made when *N*-(2-acetamido)iminodiacetic acid (ADA, $K_d$(Zn) = 83 nM, Figure 3b) was used as the metal buffer. Although the binding isotherms in both cases are fittable using the 1:1 binding equation (see the fitting curves in the insets), in our view, those numbers overestimated the zinc(II) affinity of **2** (the $K_d$ values are smaller than the true value). Citrate ($K_d$(Zn) = 12 μM) allowed the zinc(II) titration to reach saturation (Figure 3c), and the fitting of the binding isotherm gave a $K_d$ of 0.8 μM. Although based on the initial large changes in the titration data, citrate is an insufficient zinc(II) buffer for competing zinc(II) with compound **2**. On the basis of these observations, one would draw the conclusion that the apparent $K_d$ of the presumed ZnL complex is somewhere between 20 nM and 800 nM.[36] The estimates of the $K_d$ values of compounds **1, 3**, and **4** were obtained similarly and are listed in Table 4.

The pK$_a$ values of ligands **1–4** cluster in the narrow range of 4.3–4.5. Therefore, under pH neutral conditions, these compounds are in their neutral base forms. The Zn(II) sensitivity of

these compounds, therefore, shall be free of interference from pH fluctuation in the physiologically tolerated range (from 4.8 in lysosome to 7.4 of blood). Similar to other bipy-containing fluorophores that we have reported,[38,39] compounds **1–4** preferentially bind transition metal ions over alkali and alkaline earth metal ions. As expected, the selectivity of the new compounds **2** and **4** (Figures S13 and S14, Supporting Information) roughly follows the predictions of the Irving–Williams order.[40]

The contrast in photostability between *trans*-olefin **1** and configurationally locked analogue **2** is apparent in their absorption sensitivity to UV irradiation in an aqueous solution buffered at pH 7.4. When placing under the irradiation of a hand-held UV lamp ($\lambda_{ex}$ = 365 nm), the absorption band of compound **1** drops quite significantly (Figure 4a), consistent with the occurrence of a rapid photoisomerization. When a sample of **2** was subjected to the same treatment, the absorption change was rather minimal (Figure 4b). Similarly, superior photostability of **2** over **1** was observed while the ligands were saturated with $Zn(ClO_4)_2$ (Figures 4c,d). The saturation of compound **1** with zinc(II) appears to stabilize the compound against photoisomerization by a moderate extent, an interesting observation that is worthy of further investigation.

## 5. Laser Confocal Fluorescence Microscopy

The ability of **1–4** to image intracellular free zinc(II) was evaluated in live eukaryotic cells. HeLa $S_3$ cells were incubated in culture medium in the presence of a ligand (2 μM) for 30 min. The medium was removed, and the cells were rinsed twice with fresh, indicator-free medium. The cells were further incubated in the presence of sodium pyrithione (50 μM), an ionophore for facilitating zinc(II) entry through the cell membrane, and either 0 or 50 μM $ZnCl_2$ for 10 min.[41] Cell morphology was monitored by acquiring brightfield differential interference contrast (DIC) images in parallel with the fluorescence images. The lack of change in cell morphology was an indication that the indicator did not exert toxicity during the course of the incubation and the imaging experiment, which lasted over 1 h.

All fluorescence images were acquired on a confocal laser point-scanning fluorescence microscope under the excitation of a 405 nm diode laser. An emission window of 530–570 nm was selected via application of a variable bandpass filter. The images of cells stained by the configurationally locked compounds **2** or **4** are shown in Figure 5 in both fluorescence (bottom) and DIC modes (top). Using the identical instrumental parameter set, the fluorescence intensity of cells stained with either **2** or **4** in the presence of 50 μM of $ZnCl_2$ is much higher than that of the cells incubated in medium without zinc(II) supplementation. This data demonstrates the abilities of **2** and **4** in imaging zinc(II) ions in live cells. The difference in the distribution patterns highlights the inability of predicting and controlling the intracellular destinations after uptake of synthetic indicators, which has been pointed out by other researchers.[42,43]

## 6. Time-Lapse Experiments for Assessing Photostability

The photostability of the photoisomerizable compound **1** and **3** relative to that of their configurationally locked counterparts **2** and **4** in live cell fluorescence imaging experiments was assessed in the time-lapse video mode, while the fluorescence intensity of the samples

was recorded over time under constant 405 nm diode laser irradiation. Fluorescence images were selected from the video data at defined time intervals (Figures 6 and 7). The time-lapse data of cells incubated with compounds **1** and **2** under zinc(II)-enriched conditions (50 μM in the culture medium) were collected using the same set of instrumental parameters. Therefore, the decays of the fluorescence intensity originated from **1** and **2**, averaged over a number of regions of interest (ROIs), can be compared for assessing the relative photostability of these two compounds.

For both **1** and **2**, the fluorescence intensity decayed over time by visual examination (Figure 6). The intensity as a function of time is plotted in Figure 8a. It is apparent that the emission from cells loaded with compound **2** under zinc(II)-enriched conditions (50 μM $ZnCl_2$ in the growth medium) decayed slower than the cells stained with compound **1** under the identical conditions. The fluorescence images and intensity decay traces from the time-lapse experiments using **3** and **4** are shown in Figures 7 and 8b. Similarly, the configurationally immobilized **4** shows moderately but consistently higher photostability than the isomerizable counterpart **3**.

## CONCLUSION

In summary, the photostability of the charge-transfer fluoroionophore arylvinylenebipyridyls **1** and **3** is improved in their configurationally immobilized analogues **2** and **4**, respectively. The fluorescence quantum yield and lifetime measurements attribute the enhanced photostability to the reduction of the rate of nonradiative decay, presumably by blocking the photoisomerization pathway of the excited state. The brightness and zinc(II) sensitivity of the arylvinylenebipyridyls are maintained, which enable the configurationally locked compounds **2** and **4** to act as fluorescent indicators for zinc(II) ions in laser confocal microscopic imaging experiments.

## EXPERIMENTAL SECTION

### 1. Materials and General Methods

Reagents and solvents were purchased from various commercial sources and used without further purification unless otherwise stated. Spectroscopic grade solvents were used in the UV–vis and fluorescence spectroscopic measurements. All reactions were carried out in oven- or flame-dried glassware in an inert atmosphere of argon. Analytical thin-layer chromatography (TLC) was performed using precoated TLC plates with silica gel 60 F254. Flash column chromatography was performed using silica (230–400 mesh) gel as the stationary phases. ^{1}H and ^{13}C NMR spectra were acquired on 300 MHz and 500 MHz instruments, with frequencies indicated in the synthetic procedures. All chemical shifts were reported in δ units relative to tetramethylsilane. $CDCl_3$ was treated with alumina gel prior to use to remove trace acids. High resolution mass spectra (HRMS) were obtained using a time-of-flight (TOF) analyzer.

### 2. Syntheses and Characterizations

**Compound 7**—In the presence of *t*-BuOK (29 mg, 0.26 mmol), compounds **5** (271 mg, 1.38 mmol) and **6** (424 mg, 1.32 mmol) were dissolved in dry THF (10 mL) in a round-

bottom flask equipped with a magnetic stir bar. The reaction mixture was stirred overnight. Afterward, water was added to quench the reaction and the solution was partitioned between water and EtOAc. The organic layer was dried over $Na_2SO_4$ and then concentrated under reduced pressure. The crude product was fractionated on a silica gel column, and the product **7** was isolated in a 80% yield (384 mg) using $CH_2Cl_2$/EtOAc (0–30%) as the eluent. ^{1}H NMR (300 MHz, CDCl$_3$) δ/ppm 8.72 (d, $J$ = 2.3 Hz, 1H), 8.49 (s, 1H), 8.33 (d, $J$ = 8.3 Hz, 1H), 8.28 (d, $J$ = 8.1 Hz, 1H), 7.95 (dd, $J$ = 8.4, 2.3 Hz, 1H), 7.60 (dd, $J$ = 8.2, 2.2 Hz, 1H), 7.57–7.47 (m, 2H), 7.01 (d, $J$ = 16.6 Hz, 1H), 6.73 (d, $J$ = 2.5 Hz, 1H), 6.59 (dd, $J$ = 8.6, 2.5 Hz, 1H), 5.26 (s, 2H), 3.81 (s, 3H), 3.52 (s, 3H), 2.38 (s, 3H); ^{13}C NMR (75 MHz, CDCl$_3$) δ/ppm 161.0, 156.1, 154.7, 153.7, 149.8, 148.1, 137.6, 133.8, 133.3, 133.2, 127.5, 125.4, 123.2, 120.7, 120.6, 119.7, 107.5, 101.7, 95.1, 56.4, 55.6, 18.5; HRMS (CI+): calcd 363.1709 ($C_{22}H_{23}O_3N_2$ + H^{+}), found 363.1709.

**Compound 8**—TsOH·$H_2O$ (312 mg, 1.64 mmol) was added to a solution of compound **7** (300 mg, 0.828 mmol) in MeOH (10 mL) in a round-bottom flask equipped with a magnetic stir bar. The reaction mixture was stirred for overnight. The solvent was removed under reduced pressure, and the residue was washed with water, followed by trituration with ether. Compound **8** was isolated in a 90% yield (237 mg) without further purification. ^{1}H NMR (500 MHz, DMSO-$d_6$) δ/ppm 9.98 (s, 1H), 8.74 (s, 1H), 8.52 (s, 1H), 8.34 (d, $J$ = 8.3 Hz, 1H), 8.29 (d, $J$ = 8.1 Hz, 1H), 8.10 (d, $J$ = 8.5 Hz, 1H), 7.76 (d, $J$ = 8.3 Hz, 1H), 7.55 (d, $J$ = 9.1 Hz, 1H), 7.50 (d, $J$ = 16.3 Hz, 1H), 7.19 (d, $J$ = 16.6 Hz, 1H), 6.47 (s, 2H), 3.74 (s, 3H), 2.37 (s, 3H); ^{13}C NMR (125 MHz, DMSO-$d_6$) δ/ppm 160.8, 157.0, 153.8, 153.1, 150.0, 148.1, 138.0, 133.8, 133.2, 128.5, 126.4, 122.0, 120.5, 120.2, 117.0, 106.1, 101.7, 55.5, 18.3; HRMS (EI+): calcd 318.1368 ($C_{20}H_{18}N_2O_2$) found 318.1347.

**Compound 2**—To a solution of **8** (300 mg, 0.942 mmol) in THF (50 mL) in a round-bottom flask equipped with a magnetic stir bar were added anhydrous $K_2CO_3$ (651 mg, 4.71 mmol) and $I_2$ (1.2 g, 4.7 mmol). The mixture was stirred at rt for 5 h. The resulting solution was poured into a saturated $NaHCO_3$ solution (20 mL) and treated with a saturated $Na_2S_2O_3$ solution to remove the unreacted iodine. Extraction with EtOAc afforded the organic layer that was dried and concentrated. The crude solid was chromatographed on a silica gel column using EtOAc as the eluent. Compound **2** was isolated in a 95% yield (283 mg). ^{1}H NMR (300 MHz, CDCl$_3$) δ/ppm 9.10 (d, $J$ = 2.1 Hz, 1H), 8.52 (d, $J$ = 2.0 Hz, 1H), 8.44 (d, $J$ = 8.4 Hz, 1H), 8.33 (d, $J$ = 8.1 Hz, 1H), 8.18 (dd, $J$ = 8.3, 2.2 Hz, 1H), 7.64 (dd, $J$ = 8.0, 2.2 Hz, 1H), 7.48 (dd, $J$ = 8.6, 1.3 Hz, 1H), 7.10 (s, 2H), 6.90 (dd, $J$ = 8.5, 2.2 Hz, 1H), 3.89 (s, 3H), 2.41 (s, 3H); ^{13}C NMR (75 MHz, CDCl$_3$) δ/ppm 158.7, 156.4, 155.4, 153.3, 152.5, 149.8, 145.4, 137.6, 133.6, 132.2, 126.4, 122.3, 121.4, 120.8, 120.7, 112.6, 102.9, 96.0, 55.9, 18.5; HRMS (EI+): calcd 316.1212 ($C_{20}H_{16}N_2O_2$) found 316.1204.

**Compound 10[27]**—To a solution of 3-methoxythiophene **9** (1.0 g, 8.8 mmol) in THF (10 mL) at −78 °C was added $n$-BuLi (3.9 mL of 2.5 M solution in hexanes, 9.7 mmol). After stirring for 1 h, DMF (0.8 mL, 0.01 mol) was added. The solution was stirred for 1 h at rt, and water was added. The crude product 3-methoxythiophene-2-carbaldehyde **10** was obtained by extraction with $CH_2Cl_2$. The organic portions were dried over $Na_2SO_4$ before concentration under vacuum. The residue was chromatographed on silica gel using $CH_2Cl_2$

to obtain a pure product as a yellow solid in a 40% yield (500 mg). ^{1}H NMR (300 MHz, CDCl_3): δ/ppm 9.96 (s, 1H), 7.63 (d, $J$ = 5.4 Hz, 1H), 6.85 (d, $J$ = 5.4 Hz, 1H), 3.97 (s, 1H).

**Compound 11[27]**—To a solution of 3-methoxythiophene-2-carbaldehyde **10** (0.50 g, 3.5 mmol) in $CH_2Cl_2$ (20 mL) at 0 °C was added $BBr_3$ (4.2 mL of 1 M solution in heptane, 4 mmol) slowly. After being stirred for 1 day at rt, water was added to the reaction mixture. Product was extracted by $CH_2Cl_2$. After silica column chromatography, the pure product was obtained as a brown amorphous solid in a 75% yield (336 mg). ^{1}H NMR (300 MHz, CDCl_3): δ/ppm 10.72 (s, 1H), 9.64 (s, 1H), 7.60 (d, $J$ = 5.3 Hz, 1H), 6.78 (d, $J$ = 5.3 Hz, 1H).

**Compound 12**—To a solution of 3-hydroxythiophene-2-carbaldehyde **11** (336 mg, 2.63 mmol) and DIPEA (596 μL, 3.42 mmol) in THF (5 mL) at 0 °C was added MOMBr (279 μL, 3.42 mmol) over a 5 min period. The solution was stirred overnight, and then diluted with EtOAc (25 mL), washed with saturated brine (3 × 25 mL), dried over $Na_2SO_4$, and filtered. The solvent was removed under vacuum to yield an orange oil. Silica chromatography (eluted by $CH_2Cl_2$, isocratic) yielded the pure aldehyde **12** as a yellow oil in a 95% yield (430 mg). ^{1}H NMR (500 MHz, CDCl_3) δ/ppm 10.05 (s, 1H), 7.62 (d, $J$ = 5.4 Hz, 1H), 7.00 (d, $J$ = 5.4 Hz, 1H), 5.25 (s, 2H), 3.54 (s, 3H); ^{13}C NMR (125 MHz, CDCl_3) δ/ppm 181.7, 162.3, 135.0, 123.2, 118.4, 96.4, 56.9; HRMS (ESI+): calcd 195.0092 ($C_7H_8O_3S$ + $Na^+$) found 195.0100.

**Compound 13**—A flame-dried flask was charged with dry THF (20 mL) and **6** (577 mg, 1.80 mmol) and cooled to −78 °C. Compound **12** (310 mg, 1.80 mmol) and KHMDS (4.0 mL of 0.5 M in toluene, 2 mmol) were added dropwise sequentially. The mixture turned dark reddish after 15 min. The temperature was then slowly raised to rt in 2 h. The reaction mixture was poured into icy saturated brine and extracted with $CH_2Cl_2$. The organic portions were washed with saturated brine and dried over $Na_2SO_4$. The olefin product **13** as a yellow solid was obtained after fractionation on a silica column eluted by 50% EtOAc in $CH_2Cl_2$ in a 66% yield (404 mg). ^{1}H NMR (500 MHz, CDCl_3) δ/ppm 8.69 (d, $J$ = 2.2 Hz, 1H), 8.51 (dd, $J$ = 1.5, 0.7 Hz, 1H), 8.33 (d, $J$ = 8.4 Hz, 1H), 8.29 (d, $J$ = 8.1 Hz, 1H), 7.93 (dd, $J$ = 8.4, 2.3 Hz, 1H), 7.62 (dd, $J$ = 8.1, 2.2 Hz, 1H), 7.43 (d, $J$ = 16.3 Hz, 1H), 7.13 (d, $J$ = 5.5 Hz, 1H), 6.96 (d, $J$ = 5.5 Hz, 1H), 6.83 (d, $J$ = 16.3 Hz, 1H), 5.18 (s, 2H), 3.54 (s, 3H), 2.40 (s, 3H); ^{13}C NMR (125 MHz, CDCl_3) δ/ppm 154.8, 153.7, 153.1, 149.8, 147.9, 137.6, 133.4, 133.2, 133.0, 123.6, 122.3, 122.1, 120.8, 120.7, 119.3, 96.6, 56.5, 18.6; HRMS (ESI+): calcd 361.0987 ($C_{19}H_{18}N_2O_2S$ + $Na^+$) found 361.0980.

**Compound 14**—TsOH·H_2O (456 mg, 2.40 mmol) was added to a solution of compound **13** (404 mg, 1.20 mmol) in MeOH (5 mL). The reaction mixture was stirred overnight. The solvent was removed under reduced pressure, and the residue was diluted with $CH_2Cl_2$ followed by neutralization by a saturated $NaHCO_3$ solution. The organic layer was collected and concentrated under vacuum. Compound **14** was isolated via silica chromatography (eluted by 1% MeOH in $CH_2Cl_2$) as a brown solid in a 99% yield (349 mg). ^{1}H NMR (500 MHz, DMSO-d_6) δ/ppm 10.13 (s, 1H), 8.72 (d, $J$ = 2.2 Hz, 1H), 8.51 (d, $J$ = 2.2 Hz, 1H), 8.31 (d, $J$ = 8.4 Hz, 1H), 8.27 (d, $J$ = 8.1 Hz, 1H), 8.07 (dd, $J$ = 8.4, 2.2 Hz, 1H), 7.74 (dd, $J$

= 8.1, 2.2 Hz, 1H), 7.53 (d, $J$ = 16.2 Hz, 1H), 7.34 (d, $J$ = 5.4 Hz, 1H), 6.74 (d, $J$ = 16.2 Hz, 1H), 6.70 (d, $J$ = 5.4 Hz, 1H), 2.36 (s, 3H); ^{13}C NMR (125 MHz, DMSO-d$_6$) δ/ppm 154.1, 153.3, 152.6, 149.5, 147.4, 137.5, 133.4, 133.3, 132.5, 124.4, 121.4, 120.8, 120.1, 119.8, 119.4, 115.6, 17.8; HRMS (ESI+): calcd 295.0905 ($C_{17}H_{14}N_2OS + H^+$) found 295.0894.

**Compound 4**—To a solution of compound **14** (156 mg, 0.531 mmol) in THF (10 mL) were added anhydrous $K_2CO_3$ (375 mg, 2.72 mmol) and $I_2$ (691 mg, 2.72 mmol). The mixture was stirred at rt for 5 h. The resulting solution was poured into a saturated $NaHCO_3$ solution (20 mL) and treated with a saturated $Na_2S_2O_3$ solution to remove the unreacted iodine. Extraction with EtOAc afforded the organic layer that was dried and concentrated. The crude solid was chromatographed on a silica gel column using EtOAc as the eluent. Compound **4** was isolated as light yellow solid in a 95% yield (147 mg). ^{1}H NMR (500 MHz, CDCl$_3$) δ/ppm 9.05 (d, $J$ = 2.2 Hz, 1H), 8.53 (d, $J$ = 2.2 Hz, 1H), 8.43 (d, $J$ = 8.4 Hz, 1H), 8.32 (d, $J$ = 8.1 Hz, 1H), 8.12 (dd, $J$ = 8.4, 2.2 Hz, 1H), 7.65 (dd, $J$ = 8.1, 2.2 Hz, 1H), 7.26 (d, $J$ = 5.3 Hz, 1H), 7.15 (s, 1H), 7.14 (d, $J$ = 5.3 Hz, 1H), 2.42 (s, 3H); ^{13}C NMR (75 MHz, CDCl$_3$) δ/ppm 158.5, 155.2, 154.9, 153.4, 149.9, 144.9, 137.7, 133.7, 131.8, 126.9, 126.6, 125.3, 120.9, 120.8, 111.1, 102.8, 18.6; HRMS (ESI+): calcd 293.0749 ($C_{17}H_{12}N_2OS + H^+$) found 293.0750.

## 3. Zinc(II) Titration in Absorption and Emission Modes

Spectrophotometric and fluorometric titrations were conducted on a UV−vis spectrophotometer and a fluorometer, respectively, with a 1 cm semimicro quartz cuvette capped with a septum. The previously published zinc(II) titration procedure was followed.[44] The pH titration also followed a previously published procedure.[44]

## 4. Fluorescence Quantum Yield Measurements

All samples were degassed by bubbling argon through before recording the absorption and emission. Absorbance at the excitation wavelength was kept below 0.1 to minimize the inner-filter effect. The fluorescence quantum yields were determined by comparing the integrated area of the corrected emission spectrum with that of the reference quinine bisulfate ($\varphi_f$ = 0.54 in 1 N $H_2SO_4$).[45]

## 5. Fluorescence Lifetime Measurements

The lifetime values were collected using the time-correlated single photon counting (TCSPC) technique. Compounds **1–4** and their zinc(II) complexes were excited using the 370 nm LED. The LED operated at a repetition rate of 1 MHz. The data were recorded with a bandwidth of 4 nm and 10 000 counts in the peak channel. The time scale of the experiment was 100 ns (115.3 ps/channel).

## 6. Cell Culture and Confocal Fluorescence Microscopy

HeLa S$_3$ cells were seeded and grown directly in Delta T open culture dishes for at least 24 h to approximately 70–80% confluency. The culture medium was a 1:1 mixture of DMEM and Ham's F-12, supplemented with 12.5% cosmic calf serum, 0.01% (w/v) sodium pyruvate, 0.05% (w/v) L-glutamine, 0.12% (w/v) sodium bicarbonate, and 1% (v/v)

penicillin/streptomycin and finally adjusted to a pH of 7.9. In preparation for imaging, cells were rinsed twice with fresh culture medium and then incubated with the appropriate dye at a concentration of 2 μM, diluted in fresh culture medium, for 30 min at 5% $CO_2$, 95% humidity, and 37 °C. Following incubation with dye, the cells were quickly rinsed twice in fresh culture medium and then incubated with 50 μM sodium pyrithione and either 50 or 0 μM $ZnCl_2$ diluted in fresh culture medium for an additional 10 min. During this time, the Delta T culture vessel is loaded into the microscope incubation chamber stage insert.

Confocal fluorescence microscopy was performed using a confocal laser point-scanning system on an inverted microscope stand. Imaging was performed using an NA = 1.4 oil immersion objective and 405 nm diode laser line. Green fluorescence from the tested compounds was detected between 530 and 570 nm using a variable bandpass filter to isolate the waveband of interest from spectrally dispersed emission light. Video microscopy was performed using continuous acquisition at constant laser power and other settings, including the laser excitation power, PMT voltage, gain register, pixel dwell time, pixel depth, and offset. Photobleaching was evaluated by drawing an ROI around each cell, with cell boundaries determined using the brightfield DIC image and not fluorescence. Background fluorescence was determined using an ROI over part of the image not occupied by any cells and subsequently subtracted. Next, the change in absolute intensity in each ROI ($N = 21$) was determined and averaged for each time point, with representative images provided by Figures 6 and 7, and plotted in Figure 8.

## Supplementary Material

Refer to Web version on PubMed Central for supplementary material.

## ACKNOWLEDGMENTS

## REFERENCES

(1). Frederickson CJ. Int. Rev. Neurobiol. 1989; 31:145–238. [PubMed: 2689380]

(2). Vallee BL, Falchuk KH. Physiol. Rev. 1993; 73:79–118. [PubMed: 8419966]

(3). Berg JM, Shi Y. Science. 1996; 271:1081–1085. [PubMed: 8599083]

(4). Maret W. BioMetals. 2001; 14:187–190.

(5). Maret W, Li Y. Chem. Rev. 2009; 109:4682–4707. [PubMed: 19728700]

(6). Colvin RA, Holmes WR, Fontaine CP, Maret W. Metallomics. 2010; 2:306–317. [PubMed: 21069178]

(7). Hambidge M, Cousins RJ, Costello RB. J. Nutr. 2000; 130:1341S–1343S. [PubMed: 10801940]

(8). Frederickson CJ, Koh J-Y, Bush AI. Nat. Rev. Neurosci. 2005; 6:449–462. [PubMed: 15891778]

(9). Murphy, DB.; Davidson, MW. Fundamentals of Light Microscopy and Electronic Imaging. 2nd ed.. Wiley-Blackwell; Hoboken, NJ: 2013.

(10). Grynkiewicz G, Poenie M, Tsien RY. J. Biol. Chem. 1985; 260:3440–3450. [PubMed: 3838314]

(11). Minta A, Kao JPY, Tsien RY. J. Biol. Chem. 1989; 264:8171–8178. [PubMed: 2498308]

(12). Tomat E, Lippard SJ. Curr. Opin. Chem. Biol. 2010; 14:225–230. [PubMed: 20097117]

(13). Xu Z, Yoon J, Spring DR. Chem. Soc. Rev. 2010; 39:1996–2006. [PubMed: 20428518]

(14). Pluth MD, Tomat E, Lippard SJ. Annu. Rev. Biochem. 2011; 80:333–355. [PubMed: 21675918]

(15). Liu Z, He W, Guo Z. Chem. Soc. Rev. 2013; 42:1568–1600. [PubMed: 23334283]

(16). Zhu L, Yuan Z, Sreenath K, Simmons JT. RSC Adv. 2014; 4:20398–20440. [PubMed: 25071933]

(17). Lim NC, Freake HC, Brückner C. Chem.—Eur. J. 2005; 11:38–49. [PubMed: 15484196]

(18). Carol P, Sreejith S, Ajayaghosh A. Chem.—Asian J. 2007; 2:338–348. [PubMed: 17441169]

(19). Demchenko AP. J. Fluoresc. 2010; 20:1099–1128. [PubMed: 20358283]

(20). Wilson JN, Bunz UHF. J. Am. Chem. Soc. 2005; 127:4124–4125. [PubMed: 15783166]

(21). Zucchero AJ, Wilson JN, Bunz UHF. J. Am. Chem. Soc. 2006; 128:11872–11881. [PubMed: 16953627]

(22). Younes AH, Zhang L, Clark RJ, Zhu L. J. Org. Chem. 2009; 74:8761–8772. [PubMed: 19852467]

(23). Younes AH, Zhang L, Clark RJ, Davidson MW, Zhu L. Org. Biomol. Chem. 2010; 8:5431–5441. [PubMed: 20882250]

(24). Boehlow TR, Harburn JJ, Spilling CD. J. Org. Chem. 2001; 66:3111–3118. [PubMed: 11325276]

(25). Zhang L, Clark RJ, Zhu L. Chem.—Eur. J. 2008; 14:2894–2903. [PubMed: 18232042]

(26). Duan X-F, Zeng J, Zhang Z-B, Zi G-F. J. Org. Chem. 2007; 72:10283–10286. [PubMed: 18027967]

(27). Jeong Y-C, Ahn D-J, Lee W-S, Lee S-H, Ahn K-H. Bull. Korean Chem. Soc. 2011; 32:1063–1066.

(28). Suppan, P.; Ghoneim, N. Solvatochromism. The Royal Society of Chemistry; London: 1997.

(29). Painelli A, Terenziani F. J. Phys. Chem. A. 2000; 104:11041–11048.

(30). Kosower EM. Acc. Chem. Res. 1982; 15:259–266.

(31). Rettig W. Angew. Chem., Int. Ed. Engl. 1986; 25:971–988.

(32). Sissa C, Calabrese V, Cavazzini M, Grisanti L, Terenziani F, Quici S, Painelli A. Chem.—Eur. J. 2013; 19:924–935. [PubMed: 23180631]

(33). Olsen SJ. Phys. Chem. B. 2015; 119:2566–2575.

(34). To replicate the ratiometric response as shown in the titration experiments in acetonitrile, the excitation wavelength would have to be in the UV region, which would not be suitable for the following confocal fluorescence microscopy experiments

(35). Patton C, Thompson S. Epel, D. Cell Calcium. 2004; 35:427–431.

(36). Zinc(II) is able to bind bipy to form complexes of ZnL up to ZnL$_3$, depending on counter ion and/or solvent. Under metal-buffered conditions, it is conceivable that bipy binds zinc(II) together with a metal buffer ligand to form a ternary complex, which would also contribute to the observed emission and consequently the emission dependency on metal buffer. This scenario is realistic and similar to the formation of protein·zinc(II)·indicator ternary complexes that were characterized by Petering and co-workers Meeusen JW, Tomasiewicz H, Nowakowski A, Petering DH. Inorg. Chem. 2011; 50:7563–7573. [PubMed: 21774459]

(37). Kuang G-C, Allen JR, Baird MA, Nguyen BT, Zhang L, Morgan TJJ, Levenson CW, Davidson MW, Zhu L. Inorg. Chem. 2011; 50:10493–10504. [PubMed: 21905758]

(38). Sreenath K, Allen JR, Davidson MW, Zhu L. Chem. Commun. 2011; 47:11730–11732.

(39). Sreenath K, Yuan Z, Allen JR, Davidson MW, Zhu L. Chem.—Eur. J. 2015; 21:867–874. [PubMed: 25382395]

(40). Irving H, Williams RJP. Nature. 1948; 162:746–747.

(41). Forbes IJ, Zalewski PD, Hurst NP, Giannakis C, Whitehouse MW. FEBS Lett. 1989; 247:445–447. [PubMed: 2785460]

(42). Qin Y, Miranda JG, Stoddard CI, Dean KM, Galati DF, Palmer AE. ACS Chem. Biol. 2013; 8:2366–2371. [PubMed: 23992616]

(43). Maret W. Metallomics. 2015; 7:202–211. [PubMed: 25362967]

(44). Simmons JT, Allen JR, Morris DR, Clark RJ, Levenson CW, Davidson MW, Zhu L. Inorg. Chem. 2013; 52:5838–5850. [PubMed: 23621758]

(45). Fery-Forgues S, Lavabre D. J. Chem. Educ. 1999; 76:1260–1264.

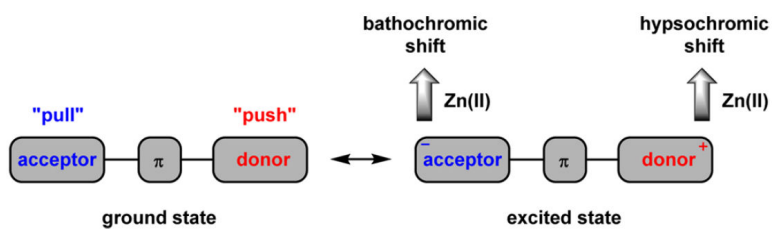**Figure 1.**
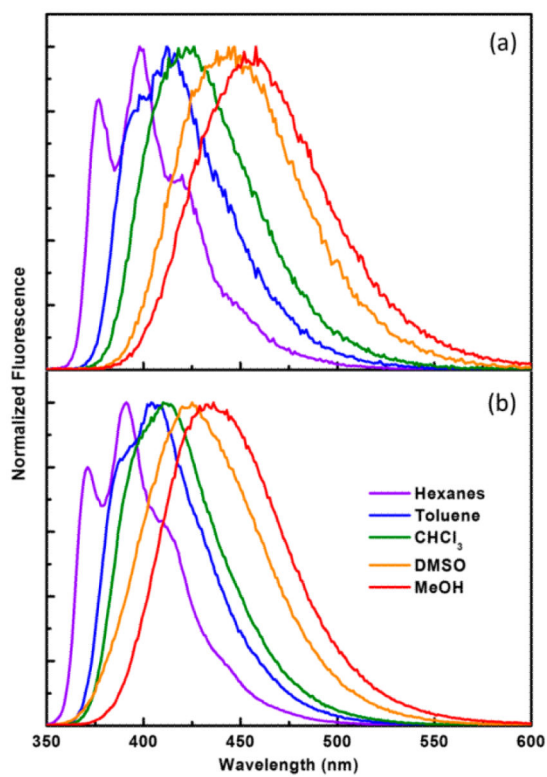Charge-transfer (or "push-pull") fluoroionophore and the effect on emission via zinc(II) coordination.

**Figure 2.**
Normalized emission spectra of (a) **2** (2.2 μM) and (b) **4** (2.5 μM) in different solvents (shown in the legend in b). $\lambda_{ex}$ = 340 nm.

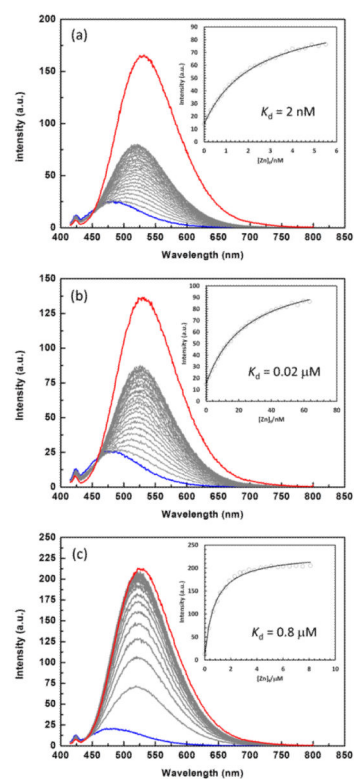**Figure 3.**
Fluorescence spectra of **2** (2.5 μM, $\lambda_{ex}$ = 405 nm) in the presence of $Zn(ClO_4)_2$ (0–2 mM) in an aqueous solution ([HEPES] = 100 mM, [metal buffer] = 1 mM, [$KNO_3$] = 100 mM, pH 7.4). Metal buffer = NTA (a); ADA (b); citrate (c). The initial zinc(II)-free and the final zinc(II)-saturated spectra of each titration experiment are coded blue and red, respectively. Insets: fluorescence intensity at indicated emission wavelength vs free zinc(II) concentration [Zn]$_f$. The solid lines are fitting curves using a 1:1 binding model.[37]
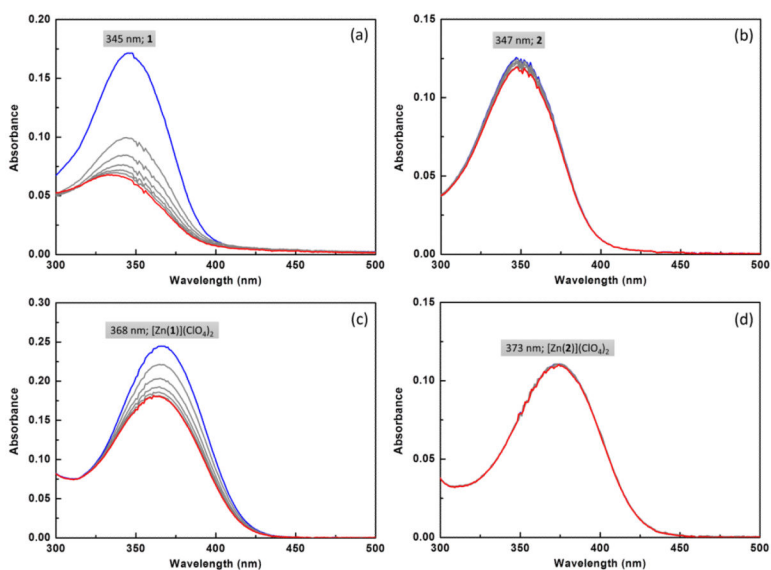
**Figure 4.**
Absorption spectra of compounds (a) **1** and (b) **2** at 5 μM each in 10% DMSO-containing aqueous solution (HEPES: 100 mM, pH = 7.4, NTA: 1 mM, KCl: 100 mM) acquired under irradiation from a hand-held UV lamp (365 nm, 4 W) for 1 min. The spectra were collected at 10 s increments from blue to red traces. The changes of absorption spectra of (c) **1** and (d) **2** under the same conditions in the presence of $Zn(ClO_4)_2$ (2 mM).
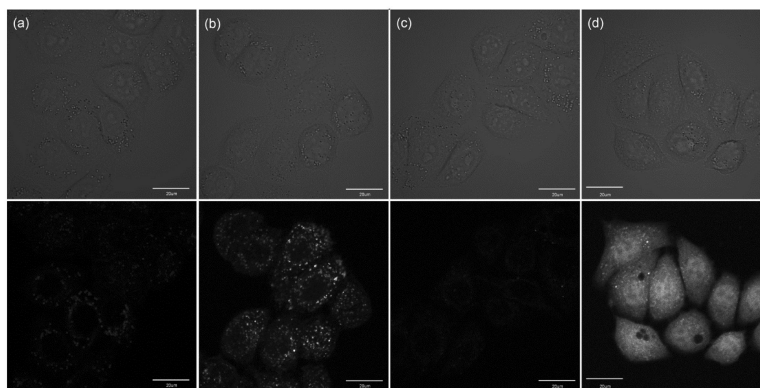
**Figure 5.**
Images of HeLa S$_3$ cells incubated with **2** (a, b) or **4** (c, d) at 2 μM for 30 min at 37 °C. The upper and lower panels are the differential interference contrast (DIC) and the fluorescence images ($\lambda_{ex}$ = 405 nm, $\lambda_{em}$ 530-570 nm), respectively. Panels a and c are images taken in the absence of supplemental zinc(II) ([ZnCl$_2$] = 0), while images in b and d are taken under zinc(II)-enriched conditions ([ZnCl$_2$] = 50 μM). [sodium pyrithione] = 50 μM. The scale bar is 20 μm.

**Figure 6.**
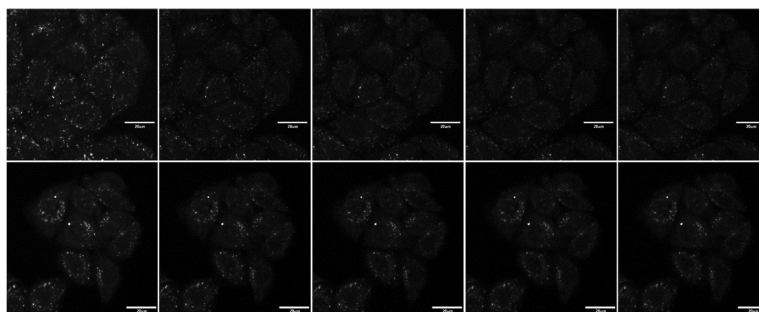Fluorescence images of HeLa S$_3$ cells ($\lambda_{ex}$ = 405 nm, emission 530–570 nm) after incubated with "unlocked" **1** (upper) or "locked" **2** (lower) at 2 μM, in the presence of ZnCl$_2$ (50 μM) and sodium pyrithione (50 μM) over time under continuous laser irradiation (images shown every 20 frames, approximately every 1 min from left to right). The scale bar is 20 μm.

**Figure 7.**
Fluorescence images of HeLa $S_3$ cells ($\lambda_{ex}$ = 405 nm, emission 530–570 nm) after incubated with "unlocked" **3** (upper) or "locked" **4** (lower) at 2 μM, in the presence of $ZnCl_2$ (50 μM) and sodium pyrithione (50 μM) over time under continuous laser irradiation (images shown every 20 frames, approximately every 1 min from left to right). The scale bar is 20 μm.
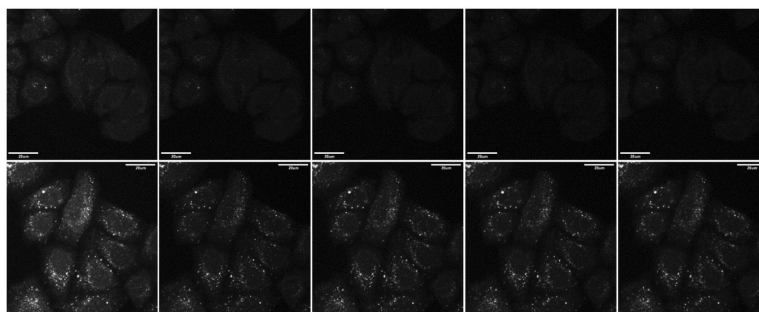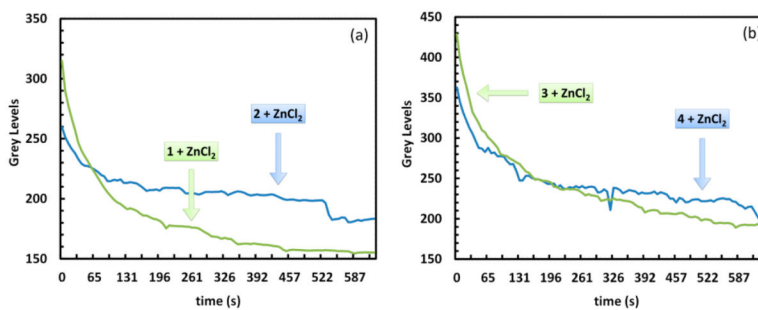
**Figure 8.**
(a) Intracellular intensity of HeLa $S_3$ cells (averaged over 21 cells, $\lambda_{ex}$ = 405 nm, $\lambda_{em}$ 530–570 nm) over time when incubated with **1** (green) or **2** (blue) at 2 μM, in the presence of $ZnCl_2$ (50 μM) and sodium pyrithione (50 μM). (b) Same comparison between **3** (green) and **4** (blue).
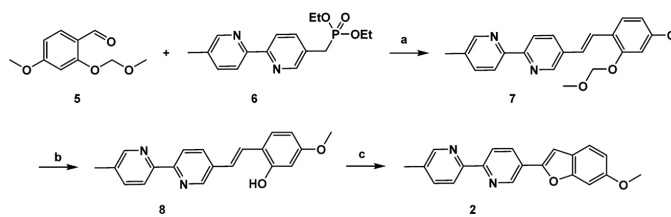
<sup>a</sup>Reagents and conditions: (a) *t*-BuOK, THF, 80%; (b) TsOH·H₂O, CH₃OH, 90%; (c) K₂CO₃, I₂, THF, 95%.

**Scheme 1.**
Synthesis of Compound 2ᵃ
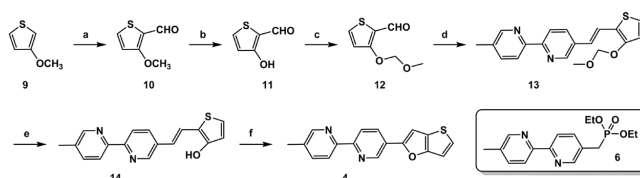
<sup>a</sup>Reagents and conditions: (a) nBuLi, DMF, 40%; (b) BBr<sub>3</sub>, CH<sub>2</sub>Cl<sub>2</sub>, 75%; (c) MOMBr, DIPEA, THF, 95%; (d) **6**, KHMDS, THF, 66%; (e) TsOH· H<sub>2</sub>O, CH<sub>3</sub>OH, 99%; (f) K<sub>2</sub>CO<sub>3</sub>, I<sub>2</sub>, THF, 95%.

**Scheme 2.**
Synthesis of Compound 4[a]

**Chart 1.**
Structures of AVBs

**Table 1**

Fluorescence Quantum Yield ($\varphi$), Lifetime ($\tau$), and Radiative and Nonradiative Decay Rate Constants ($k_r$ and $k_{nr}$) of Compounds 1 and 2 in Different Solvents[a]
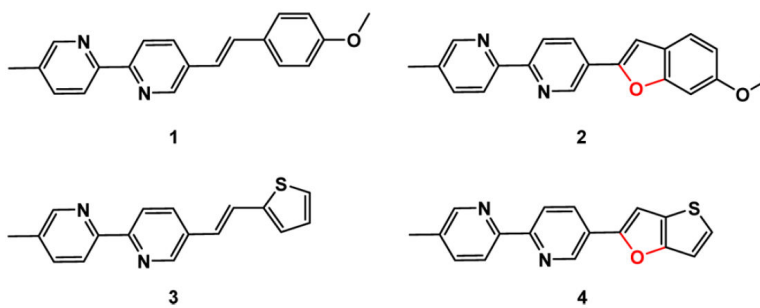
| solvent | $\varepsilon$ | $\varphi$ (1) | $\varphi$ (2) | $\tau$/ns (1) | $\tau$/ns (2) | $k_r$/ns$^{-1}$ (1) | $k_r$/ns$^{-1}$ (2) | $k_{nr}$/ns$^{-1}$ (1) | $k_{nr}$/ns$^{-1}$ (2) |
|---|---|---|---|---|---|---|---|---|---|
| hexanes | 2.02 | 0.60 | 0.84 | 0.91 | 1.12 | 0.65 | 0.75 | 0.43 | 0.14 |
| dioxane | 2.3 | 0.49 | 0.78 | 0.84 | 1.47 | 0.60 | 0.53 | 0.59 | 0.15 |
| benzene | 2.3 | 0.53 | 0.75 | 0.75 | 1.30 | 0.71 | 0.58 | 0.62 | 0.19 |
| toluene | 2.4 | 0.54 | 0.71 | 0.79 | 1.28 | 0.69 | 0.55 | 0.56 | 0.23 |
| CHCl$_3$ | 4.8 | 0.36 | 0.70 | 0.70 | 1.57 | 0.52 | 0.45 | 0.90 | 0.19 |
| EtOH | 25 | 0.35 | 0.83 | 0.92 | 2.02 | 0.39 | 0.41 | 0.69 | 0.08 |
| MeOH | 33 | 0.33 | 0.79 | 0.95 | 2.18 | 0.35 | 0.36 | 0.69 | 0.08 |
| MeCN | 36.6 | 0.28 | 0.91 | 0.60 | 1.84 | 0.47 | 0.49 | 1.20 | 0.05 |
| DMF | 38.3 | 0.37 | 0.69 | 0.76 | 1.80 | 0.48 | 0.38 | 0.82 | 0.17 |
| DMSO | 47 | 0.48 | 0.82 | 0.86 | 1.80 | 0.56 | 0.46 | 0.59 | 0.10 |
| H$_2$O[b] | 78.5 | 0.05 | 0.25 | 1.11 | 2.48 | 0.04 | 0.10 | 0.86 | 0.30 |

[a] $\varepsilon$: dielectric constant; $\varphi$: fluorescence quantum yield; $\tau$: fluorescence lifetime determined via time-correlated single-photon counting (TCSPC); $k_r$ and $k_{nr}$: radiative and nonradiative decay time constants, determined using eqs 1 and 2. The table is sorted in the ascending order of $\varepsilon$.

[b] An aqueous solution buffered by HEPES (100 mM) at pH 7.4.

**Table 2**

Fluorescence Quantum Yield ($\varphi$), Lifetime ($\tau$), and Radiative and Nonradiative Decay Rate Constants ($k_r$ and $k_{nr}$) of Compounds 3 and 4 in Different Solvents[a]

| solvent | ε | φ (3) | φ (4) | τ/ns (3) | τ/ns (4) | $k_r$/ns$^{-1}$ (3) | $k_r$/ns$^{-1}$ (4) | $k_{nr}$/ns$^{-1}$ (3) | $k_{nr}$/ns$^{-1}$ (4) |
|---|---|---|---|---|---|---|---|---|---|
| hexanes | 2.02 | 0.16 | 0.50 | 0.46 | 0.85 | 0.35 | 0.59 | 1.83 | 0.59 |
| dioxane | 2.3 | 0.10 | 0.50 | 0.41 | 0.94 | 0.24 | 0.53 | 2.20 | 0.53 |
| benzene | 2.3 | 0.10 | 0.59 | 0.40 | 0.85 | 0.25 | 0.69 | 2.25 | 0.48 |
| toluene | 2.4 | 0.12 | 0.58 | 0.43 | 0.86 | 0.28 | 0.67 | 2.05 | 0.49 |
| CHCl$_3$ | 4.8 | 0.07 | 0.44 | 0.34 | 0.92 | 0.21 | 0.48 | 2.74 | 0.61 |
| EtOH | 25 | 0.05 | 0.66 | 0.33 | 1.63 | 0.15 | 0.40 | 2.88 | 0.21 |
| MeOH | 33 | 0.04 | 0.65 | 0.32 | 1.82 | 0.13 | 0.36 | 3.00 | 0.19 |
| MeCN | 36.6 | 0.04 | 0.60 | 0.23 | 1.30 | 0.17 | 0.46 | 4.17 | 0.31 |
| DMF | 38.3 | 0.06 | 0.67 | 0.32 | 1.34 | 0.19 | 0.50 | 2.94 | 0.25 |
| DMSO | 47 | 0.07 | 0.76 | 0.33 | 1.51 | 0.21 | 0.50 | 2.82 | 0.16 |
| H$_2$O[b] | 78.5 | 0.06 | 0.54 | 0.30 | 2.31 | 0.20 | 0.23 | 3.13 | 0.20 |

[a] ε: dielectric constant; φ: fluorescence quantum yield; τ: fluorescence lifetime determined via time-correlated single-photon counting (TCSPC); $k_r$ and $k_{nr}$: radiative and nonradiative decay constants, determined using eqs 1 and 2. The table is sorted in the ascending order of ε.

[b] An aqueous solution buffered by HEPES (100 mM) at pH 7.4.

**Table 3**

Photophysical Parameters of 1–4 (L) and Their Zinc(II) Complexes (ZnL) in CH$_3$CN[a]

| L | $\lambda_{abs(L)}$ (nm) | $\lambda_{abs(ZnL)}$ (nm) | $\varphi_L$ | $\varphi_{ZnL}$ | $\lambda_{em(L)}$ (nm) | $\lambda_{em(ZnL)}$ (nm) | $\Delta\tilde{\nu}_{em}\ (cm^{-1})$ | $\tau_L$ (ns) | $\tau_{ZnL}$ (ns) | $k_{r(L)}$ (ns$^{-1}$) | $k_{r(ZnL)}$ (ns$^{-1}$) | $k_{nr(L)}$ (ns$^{-1}$) | $k_{nr(ZnL)}$ (ns$^{-1}$) |
|---|---|---|---|---|---|---|---|---|---|---|---|---|---|
| 1 | 345 | 374 | 0.28 | 0.46 | 431 | 533 | 4440 | 0.60 | 3.14 | 0.47 | 0.15 | 1.20 | 0.17 |
| 2 | 347 | 381 | 0.91 | 0.34 | 435 | 538 | 4401 | 1.84 | 3.33 | 0.49 | 0.10 | 0.05 | 0.20 |
| 3 | 348 | 375 | 0.04 | 0.25 | 422 | 504 | 3855 | 0.23 | 1.91 | 0.17 | 0.13 | 4.17 | 0.39 |
| 4 | 343 | 380 | 0.60 | 0.55 | 420 | 505 | 4008 | 1.30 | 3.71 | 0.46 | 0.15 | 0.31 | 0.12 |

[a]$\lambda_{abs(L)}$ and $\lambda_{abs(ZnL)}$ are wavelengths at absorbance maxima; $\varphi_L$ and $\varphi_{ZnL}$ are fluorescence quantum yields $\lambda_{em(L)}$ and $\lambda_{em(ZnL)}$ are wavelengths at emission maxima; $\Delta\tilde{\nu}_{em}$ is the zinc(II)-binding caused emission frequency shift in cm$^{-1}$; $\tau_L$ and $\tau_{ZnL}$ are fluorescence lifetimes; $k_r$ and $k_{nr}$ are calculated from eqs 1 and 2.

**Table 4**

Photophysical Parameters of Ligands (L) 1–4 and Their Zinc(II) Complexes [ZnL](ClO$_4$)$_2$ in a Neutral Aqueous Solution[a]

| L | $\lambda_{abs(L)}$ (nm) | $\lambda_{abs(ZnL)}$ (nm) | $\Phi_L$ | $\Phi_{ZnL}$ | $\lambda_{em(L)}$ (nm) | $\lambda_{em(ZnL)}$ (nm) | $\tau_L$ (ns) | $\tau_{ZnL}$ (ns) | $k_{r(L)}$ (ns$^{-1}$) | $k_{r(ZnL)}$ (ns$^{-1}$) | $k_{nr(L)}$ (ns$^{-1}$) | $k_{nr(ZnL)}$ (ns$^{-1}$) | $K_d$ (μM) | p$K_a$ |
|---|---|---|---|---|---|---|---|---|---|---|---|---|---|---|
| 1 | 344 | 368 | 0.05 | 0.31 | 460 | 513 | 1.11 | 2.69 | 0.04 | 0.12 | 0.86 | 0.26 | 0.04–2 | 4.5 |
| 2 | 347 | 373 | 0.25 | 0.15 | 478 | 524 | 2.48 | 2.42 | 0.10 | 0.06 | 0.30 | 0.35 | 0.02–0.8 | 4.3 |
| 3 | 350 | 371 | 0.06 | 0.18 | 456 | 493 | 0.30 | 1.75 | 0.20 | 0.10 | 3.13 | 0.47 | 0.009–0.2 | 4.3 |
| 4 | 347 | 372 | 0.54 | 0.44 | 459 | 495 | 2.31 | 3.29 | 0.23 | 0.13 | 0.20 | 0.17 | 0.01–0.4 | 4.3 |

[a] $\varphi$L and $\varphi$ZnL are the fluorescence quantum yields in zinc(II)-free and -saturated forms, respectively; $\tau_L$ and $\tau_{ZnL}$ are the fluorescence lifetimes; $k_r$ and $k_{nr}$ are calculated from eqs 1 and 2; $K_d$ is the dissociation constant of a presumed ZnL complex; $K_a$ is the acidity constant of the conjugate acid of the ligand. All data except p$K_a$ were measured in an aqueous solution buffered by HEPES (100 mM) at pH 7.4.